Effects of spectral entanglement in polarization-entanglement swapping and type-I fusion gates

Travis S. Humble* and Warren P. Grice†

Center for Engineering Science Advanced Research, Computer Science and Mathematics Division, Oak Ridge National Laboratory, Oak Ridge, Tennessee 37831-6015, USA

(Received 10 October 2007; published 11 February 2008)

We examine how spectral entanglement in polarization-entangled photon states generated from bulk-crystal, spontaneous parametric down-conversion affects the success of entanglement swapping and type-I fusion gates. We quantify the success of the entanglement swapping and fusion gates by calculating the bipartite concurrence and residual tangle, respectively, in terms of the joint spectral probability amplitudes of the initial broad-bandwidth polarization-entangled states. We find that both polarization-entanglement measures depend strongly on the initial spectral entanglement, as well as on the configuration of the independent sources. Specifically, when spectral differences correlate with polarization, the optimal source configuration is different for the two protocols. We conclude that this distinction is founded in how the underlying Bell-state measurement and quantum-erasure techniques respond differently to distinguishing spectral information.

DOI: 10.1103/PhysRevA.77.022312 PACS number(s): 03.67.Mn, 03.65.Ud, 42.50.Dv, 42.65.Lm

I. INTRODUCTION

Polarization-entangled photon pairs are a widely used resource for demonstrating quantum information protocols. Their use is promoted by the relatively bright sources of entangled photons derived from spontaneous parametric down-conversion (SPDC), as well as the ease with which qubits of information can be encoded into polarization states [1]. However, polarization-encoded qubits are also characterized by the spectral and spatial modes they occupy. While not the primary carriers of quantum information, these adjunct spatial and spectral degrees of freedom affect the experimental realization of polarization-based protocols. In particular, correlations within these adjunct degrees of freedom often serve as distinguishing information that is not erasable by straightforward mode-matching efforts, as shown recently for the case of quantum teleportation [2]. In SPDC the strongly correlated frequencies of the down-converted photons lead to spectral entanglement in the joint probability amplitude that can distinguish the photons even when their marginal spectra appear identical [3,4]. Similarly, conservation of momentum leads to correlations between the wave vectors of the down-converted photon pair that can distinguish the photons in terms of their spatial modes [5]. Additional forms of potentially distinguishing information arise when the spatial, spectral, and polarization properties are correlated with one another [2,4,6–8].

In practice, spatial and spectral entanglement is removed by filtering the spatial and spectral modes, e.g., using single-mode fibers and narrow-bandwidth spectral filters. However, a significant drawback to this approach is that the number of detected photons is significantly reduced (relative to the number of generated pairs). While filtering works well for demonstrating proof of principle experiments, it is largely impractical for more elaborate protocols that require many polarization-entangled photons. The alternative of directly generating photons that are unentangled in the non-information-carrying degrees of freedom approaches the polarization-encoded qubits often idealized in the theoretical and experimental literature. Various techniques for achieving this ideal have been proposed [6,7,9–12]. An accompanying issue is to what extent the adjunct degrees of freedom must be engineered as indistinguishable to achieve a given level of fidelity. The answer to this question appears to depend on the application setting for which the source is designed. For example, whereas correlations between the spectral and polarization degrees of freedom diminish the visibility in a two-photon polarization-correlation experiment [6], the same correlations optimize the sought-after interference in the Hong-Ou-Mandel experiment [6,8]. Moreover, simultaneous entanglement in multiple degrees of freedom can also enable alternatives to exclusively polarization-based technique. In the latter context, the photon pair is characterized as being hyperentangled with respect to multiple degrees of freedom [13,14]. The case of embedded Bell-state analysis is one recent example of how hyperentanglement can greatly improve the efficiency of a protocol or measurement [15,16].

In the present paper, we examine how spectral entanglement in polarization-entangled photon pairs impacts the success of two polarization-based, two-qubit gates common to strategies for quantum computing: entanglement swapping and type-I fusion. Entanglement swapping [17] is central to the offline preparations in the quantum circuit modeled advanced by Knill, LaFlamme, and Milburn [18]. It is also a key component in the notion of a quantum repeater [19]. The type-I fusion gate [20], which is also a parity-check gate [21], was proposed by Browne and Rudolph as a means for preparing polarization-encoded linear cluster states, i.e., the multiqubit entangled states that are prerequisites for the one-way quantum computing approach of Raussendorf and Briegel [22,23]. We establish the connection between the effectiveness of these protocols and the spectral entanglement carried by the underlying polarization-entangled photons. We begin by introducing in Sec. II notation for the spectrally multimode, polarization-entangled states prepared from SPDC sources. In Sec. III, the success of entanglement swapping is quantified by calculating the bipartite concurrence in

*humblets@ornl.gov
†gricew@ornl.gov

 ©2008 The American Physical Society

terms of the initial joint spectral probability amplitudes for the case of four distinct source configurations. Similarly, type-I fusion is analyzed in Sec. IV for the case of two incident photon pairs and the gate success is quantified in terms of the residual entanglement of the tripartite cluster state. In Sec. V, the results of the preceding sections are extended to a particular case of making multiple sequential calls to each protocol, and conclusions are drawn in Sect. VI by comparing results for the two gates.

II. BIPHOTON STATE

The spectrally multimode, polarization-entangled state of photons 1 and 2

$$|\varphi_{12}\rangle = \frac{1}{\sqrt{2}}\int d\omega \int d\omega'[f_{12}(\omega,\omega')|h_1(\omega),v_2(\omega')\rangle + g_{12}(\omega,\omega')|v_1(\omega),h_2(\omega')\rangle], \quad (1)$$

describes the spatially filtered output from either a type-II SPDC, cross-ringed configuration [24] or a type-I SPDC, twin-crystal configuration [25].[1] The horizontally and vertically polarized modes of the jth photon are denoted as $|h_j(\omega)\rangle = h_j^\dagger(\omega)|\text{vac}\rangle$ and $|v_j(\omega)\rangle = v_j^\dagger(\omega)|\text{vac}\rangle$, respectively. Although Eq. (1) resembles a spectrally multimode extension of a single-mode, polarization-encoded Bell state, this analogy fails when the joint spectral probability amplitudes $f_{12}(\omega,\omega')$ and $g_{12}(\omega,\omega')$ are not separable from the corresponding polarization degrees of freedom. In addition, while we assume equally weighted probabilities

$$\int d\omega \int d\omega' |f_{12}(\omega,\omega')|^2 = \int d\omega \int d\omega' |g_{12}(\omega,\omega')|^2 = 1, \quad (2)$$

the joint spectra are not required to be identical.

Two specific relationships between the joint spectral amplitudes are most relevant to current experimental work. In the first case, illustrated by Fig. 1(a), the joint spectral amplitudes satisfy the identity

$$f_{12}^{\text{pol}}(\omega,\omega') = g_{12}^{\text{pol}}(\omega',\omega), \quad (3)$$

in which case the marginal spectra of the photons correlate with the polarization degree of freedom. Physically, this relationship arises in type-II SPDC, where oppositely polarized photons propagate through a birefringent crystal. In the second case, spectral differences correlate with path and the joint spectra satisfy

$$f_{12}^{\text{path}}(\omega,\omega') = g_{12}^{\text{path}}(\omega,\omega'), \quad (4)$$

as illustrated by Fig. 1(b). States satisfying Eq. (4) are produced from a type-II medium by using post-production linear optics to transform the down-conversion output so that the joint amplitudes are identical [27]. Additionally, identical joint spectral amplitudes can serve as a reasonable approximation to the entangled states prepared directly by a type-I SPDC, twin-crystal source [1]. However, this approximation fails to account for the distinct walk-off and dispersion effects that arise in the separate crystals [25]. Note that when Eq. (4) is satisfied the biphoton state is hyperentangled, i.e., the photons are entangled in the polarization and spectral degrees of freedom with the degree of entanglement in the latter depending on the separability of the joint spectral amplitude. In contrast, the biphoton state generally cannot be factorized into a product of spectral and polarization amplitudes when the joint spectral amplitudes satisfy Eq. (3).

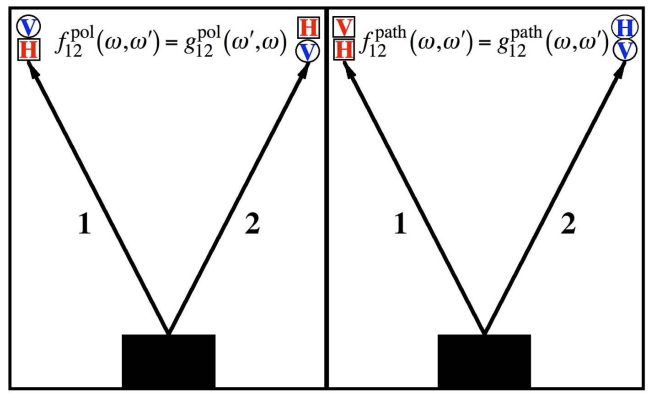

FIG. 1. (Color online) A comparison of how spectral properties correlate with polarization (left panel) and spatial degrees of freedom (right panel). Boxes (red) and circles (blue) indicate the different marginal spectra for the horizontal (H) and vertical (V) polarization states. The inset relationships define the different types of correlations. The black boxes signify entanglement sources and any additional linear optical elements.

Broad-bandwidth pumping of a degenerate SPDC source produces a joint spectral amplitude well approximated by the Gaussian form [2–4,6]

$$f_{12}(\omega,\omega') = N\exp\left[-\frac{1}{2(1-\mu^2)}\left(\frac{\Delta\omega^2}{\sigma^2} - \frac{2\mu\Delta\omega\Delta\omega'}{\sigma\sigma'} + \frac{\Delta\omega'^2}{\sigma'^2}\right)\right], \quad (5)$$

where the difference frequencies $\Delta\omega = \omega - \omega_0$ and $\Delta\omega' = \omega' - \omega_0$ are defined relative to half the pump-pulse frequency $2\omega_0$ and the normalization constant N is defined by $N^{-2} = \pi\sigma\sigma'\sqrt{1-\mu^2}$. Definitions for the linear correlation μ and the marginal bandwidths σ and σ' in terms of experimental parameters are found in Refs. [2,4].

To investigate the entanglement carried by the joint spectral amplitude, we use the Schmidt decomposition [26]

$$f_{12}(\omega,\omega') = \sum_{n=0}^{\infty} \lambda_n^{1/2} u_n(\Delta\omega) v_n(\Delta\omega'), \quad (6)$$

where the nth pair of Schmidt modes $u_n(\omega)$ and $v_n(\omega')$, each belong to a complete set of orthonormal functions and the nonnegative Schmidt coefficients λ_n are normalized to unity. The Schmidt number

[1] Equating type-I SPDC output with Eq. (1) requires rotating the polarization in one of the spatial paths.

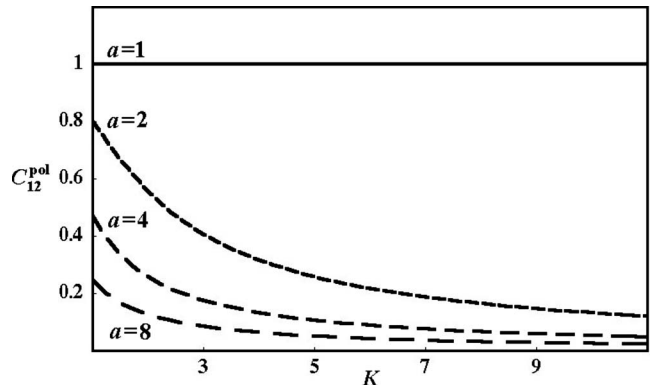

FIG. 2. The concurrence of photon pair (1,2) as a function of the spectral entanglement K when spectral differences correlate with polarization. The curves are labeled according to the value of the aspect ratio $a=\sigma/\sigma'$.

$$K = 1 \Big/ \sum_{n=0}^{\infty} \lambda_n^2 \tag{7}$$

quantifies the spectral entanglement [28]: in the absence of spectral entanglement, the single nonzero Schmidt coefficient is unity and $K=1$, while $K>1$ is indicative of a spectrally entangled joint probability amplitude.

The nth pair of Schmidt modes for Eq. (5) are $u_n(\omega) = h_n^{\sigma\sqrt{1-\mu^2}}(\omega)$ and $v_n(\omega') = h_n^{\sigma'\sqrt{1-\mu^2}}(\omega')$, where

$$h_n^{\alpha}(x) = e^{-x^2/2\alpha^2} H_n(x/\alpha)/\sqrt{\alpha\pi^{1/2}2^n n!} \tag{8}$$

is the normalized Hermite function and $H_n(x)$ is the nth Hermite polynomial [29]. The Schmidt coefficients are

$$\lambda_n = \operatorname{sech}^2 \varphi \tanh^{2n} \varphi, \tag{9}$$

where the angle φ is related to the linear correlation by $\mu = \tanh 2\varphi$, and the Schmidt number evaluates to

$$K = \cosh 2\varphi, \tag{10}$$

which monotonically increases as the linear correlation μ approaches ± 1.

To quantify polarization entanglement, the polarization state of Eq. (1) is obtained by tracing over the total biphoton density matrix with respect to the spectral degrees of freedom

$$\tilde{\rho}_{12} = \frac{1}{2}(|h_1,v_2\rangle\langle h_1,v_2| + G_{12}|h_1,v_2\rangle\langle v_1,h_2| + G_{12}^*|v_1,h_2\rangle\langle h_1,v_2| + |v_1,h_2\rangle\langle v_1,h_2|), \tag{11}$$

where the off-diagonal coherence element is

$$G_{12} = \int d\omega \int d\omega' f_{12}(\omega,\omega') g_{12}(\omega,\omega')^*. \tag{12}$$

A measure of the polarization entanglement of $\tilde{\rho}_{12}$ is the concurrence C_{12}, which is defined for a discrete bipartite state as $C_{12}=\max\{0,\varepsilon_1-\varepsilon_2-\varepsilon_3-\varepsilon_4\}$ [30]. The ε_i's (with $\varepsilon_1 \geqslant \varepsilon_2 \geqslant \varepsilon_3 \geqslant \varepsilon_4$) are the square roots of the eigenvalues of $\tilde{\rho}_{12}(\sigma_{1y}\otimes\sigma_{2y})\tilde{\rho}_{12}^*(\sigma_{1y}\otimes\sigma_{2y})$, where $\sigma_{1y}=i|v_1\rangle\langle h_1|-i|h_1\rangle\langle v_1|$ and $\sigma_{2y}=i|v_2\rangle\langle h_2|-i|h_2\rangle\langle v_2|$. Diagonalization yields

$$\varepsilon_1 = \frac{1+|G_{12}|}{2}$$

$$\varepsilon_2 = \frac{1-|G_{12}|}{2}, \tag{13}$$

and $\varepsilon_3=\varepsilon_4=0$, from which it follows that the concurrence of $\tilde{\rho}_{12}$ is $C_{12}=|G_{12}|$.

It follows from Eq. (12) that when the joint spectra are identical the concurrence C_{12} is maximal and independent of the spectral entanglement. This is because the spectral and polarization degrees of freedom are uncoupled from one another. In contrast, when spectral properties correlate with polarization, the concurrence of the polarization-entangled state depends on the overlap of the joint spectral amplitudes and, consequently, on the spectral entanglement. In terms of the Schmidt decomposition, the polarization coherence can be written as

$$G_{12} = \sum_{m,n=0}^{\infty} \sqrt{\lambda_m \lambda_n} L_{mn} L_{nm}^*, \tag{14}$$

where

$$L_{mn} = \int u_m(\omega) v_n(\omega)^* d\omega \tag{15}$$

is an interference integral between the Schmidt modes, i.e., an overlap between single-photon spectral states. For the Gaussian joint spectral amplitude, the concurrence in this case explicitly evaluates to

$$C_{12}^{\text{pol}} = \frac{2a}{\sqrt{(a^2-1)^2K^2+4a^2}}, \tag{16}$$

where we introduce the aspect ratio $a=\sigma/\sigma'$. In Fig. 2 C_{12}^{pol} is plotted as a function of the spectral entanglement K for dif-

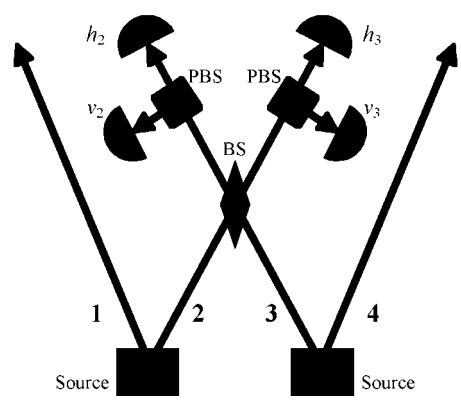

FIG. 3. An entanglement swapping experiment, where the interference of photons 2 and 3 at a 50:50 beam splitter (BS) is analyzed using two polarization beam splitters (PBS) and four detectors (h_2, v_2, h_3, and v_3). Certain coincidences between detectors (semicircles) signal the projection of photons 1 and 4 into a Bell state. Black boxes signify entanglement sources and any additional linear optical elements.

ferent values of a. As K approaches infinity the concurrence vanishes because the photons become completely distinguishable with respect to frequency. The concurrence is largest when $K=1$, but only maximal when the spectral modes are also matched, i.e., $a=1$.

III. ENTANGLEMENT SWAPPING

In this section, we calculate the concurrence obtainable from the entanglement-swapping setup shown in Fig. 3. A four-photon pure state $|\Psi_{1234}\rangle=|\varphi_{12}\rangle|\varphi_{34}\rangle$ is prepared from two independent sources with the state of photons 3 and 4 defined analogous to Eq. (2). After photons 2 and 3 interfere at a 50:50 beam splitter, they are sent to a polarization-resolving detection apparatus that effectively performs a partial Bell-state measurement [31]. The output of the 50:50 beam splitter is defined by the unitary transformations

$$B_{23}^{\dagger}h_2B_{23}=\frac{1}{\sqrt{2}}(h_2+ih_3),$$

$$B_{23}^{\dagger}h_3B_{23}=\frac{1}{\sqrt{2}}(h_3+ih_2), \tag{17}$$

with similar equations holding for v_2 and v_3. The coincidence detection events following the beam splitter are modeled to account for the spectral and polarization degrees of freedom [32]. We assume the photon bandwidth is narrow relative to the resolution of the detectors, so that coincidences between detectors, e.g., h_2 and v_2, can be modeled by the projection operator

$$\Pi(h_2,v_2)=\int d\omega\int d\omega'|h_2(\omega),v_2(\omega')\rangle\langle h_2(\omega),v_2(\omega')|, \tag{18}$$

where for simplicity we have assumed unit detector efficiencies.

The state of photons 1 and 4 following detection is, e.g.,

$$\rho_{14}=\mathrm{Tr}_{23}[\Pi(h_2,v_2)B_{23}\rho_{1234}B_{23}^{\dagger}\Pi(h_2,v_2)], \tag{19}$$

where $\rho_{1234}=|\Psi_{1234}\rangle\langle\Psi_{1234}|$ and the trace is over all the degrees of freedom of photons 2 and 3. We obtain for the un-normalized state

$$\begin{aligned}\rho_{14}=\frac{1}{16}\int d\omega\int d\omega'\int d\omega''\int d\omega'''\int d\bar{\omega}\int d\bar{\omega}'\{&f_{12}(\omega,\bar{\omega}')f_{34}(\bar{\omega},\omega'')f_{12}(\omega',\bar{\omega}')^*f_{34}(\bar{\omega},\omega''')^*|h_1(\omega),v_4(\omega'')\rangle\langle h_1(\omega'),v_4(\omega''')|\\&+f_{12}(\omega,\bar{\omega}')f_{34}(\bar{\omega},\omega'')g_{12}(\omega',\bar{\omega})^*g_{34}(\bar{\omega}',\omega''')^*|h_1(\omega),v_4(\omega'')\rangle\langle v_1(\omega'),h_4(\omega''')|\\&+g_{12}(\omega,\bar{\omega})g_{34}(\bar{\omega}',\omega'')f_{12}(\omega',\bar{\omega}')^*f_{34}(\bar{\omega},\omega''')^*|v_1(\omega),h_4(\omega'')\rangle\langle h_1(\omega'),v_4(\omega''')|\\&+g_{12}(\omega,\bar{\omega})g_{34}(\bar{\omega}',\omega'')g_{12}(\omega',\bar{\omega})^*g_{34}(\bar{\omega}',\omega''')^*|v_1(\omega),h_4(\omega'')\rangle\langle v_1(\omega'),h_4(\omega''')|\}.\end{aligned} \tag{20}$$

An identical expression holds for the biphoton state following coincidences at detectors (h_3, v_3), while coincidences at either (h_2, v_3) or (h_3, v_2) lead to an overall minus sign in the off-diagonal terms [33].

The normalized polarization density matrix of photons 1 and 4 is

$$\begin{aligned}\tilde{\rho}_{14}=\frac{1}{2}(&|h_1,v_4\rangle\langle h_1,v_4|+G_{14}|h_1,v_4\rangle\langle v_1,h_4|\\&+G_{14}^{*}|v_1,h_4\rangle\langle h_1,v_4|+|v_1,h_4\rangle\langle v_1,h_4|),\end{aligned} \tag{21}$$

where

$$\begin{aligned}G_{14}=\int d\omega\int d\omega'\int d\bar{\omega}\int d\bar{\omega}'f_{12}(\omega,\bar{\omega}')g_{34}(\bar{\omega}',\omega')^*\\\times g_{12}(\omega,\bar{\omega})^*f_{34}(\bar{\omega},\omega').\end{aligned} \tag{22}$$

The concurrence of $\tilde{\rho}_{14}$ immediately follows by analogy with Eq. (13), i.e., $C_{14}=|G_{14}|$.

We consider how C_{14} varies with the different source configurations in Fig. 4. In source configuration (a), spectral differences correlate with polarization and $f_{12}^{\mathrm{pol}}(\omega,\omega')=f_{34}^{\mathrm{pol}}(\omega,\omega')$. Substituting the Gaussian approximation for this common joint amplitude into Eq. (22) yields a concurrence

$$C_{14}^{(a)}=\frac{2a}{(a^2+1)K}, \tag{23}$$

where again $a=\sigma/\sigma'$. As expected, the concurrence after entanglement swapping is never greater than the initial entanglement of either photon pair, cf. Eq. (16). Plots of Eq. (23) versus K in the upper panel of Fig. 5 show that the concurrence will peak in the absence of spectral entanglement, i.e., for $K=1$, while for nonzero spectral entanglement we have $C_{14}<C_{12}$. For comparison, reconfiguring the sources as depicted in configuration (b), so that $f_{12}^{\mathrm{pol}}(\omega,\omega')=f_{34}^{\mathrm{pol}}(\omega',\omega)$, generally yields a lower concurrence

$$C_{14}^{(b)}=\frac{4a^2}{(a^2+1)K\sqrt{(a^2-1)^2K+4a^2}}, \tag{24}$$

which is plotted in the lower panel of Fig. 5.

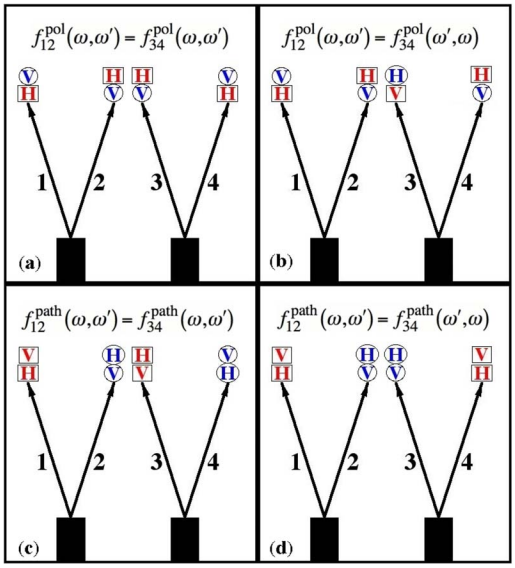

FIG. 4. (Color online) Four configurations of entanglement sources distinguished by the relationships between the joint spectral amplitudes. Boxes (red) and circles (blue) denote the different marginal spectra of the horizontal (H) and vertical (V) polarization states. In (a) and (b) spectral differences correlate with polarization, while in (c) and (d) spectral differences correlate with path. Black boxes signify entangled photon sources and any additional linear optical elements.

There are two cases of interest when the joint spectra are uncoupled from polarization and spectral differences correlate with path. First, when $f_{12}^{path}(\omega,\omega')=f_{34}^{path}(\omega,\omega')$, as in source configuration (c), the concurrence $C_{14}^{(c)}$ equals $C_{14}^{(a)}$, and the upper panel of Fig. 5 plots the corresponding dependence on spectral entanglement for this case. For the source configuration in (d), $f_{12}^{path}(\omega,\omega')=f_{34}^{path}(\omega',\omega)$ and the concurrence evaluates to

$$C_{14}^{(d)} = \sqrt{1-\mu^2} = 1/K. \tag{25}$$

Because the interfering photons are mode matched in this last source configuration, the obtainable concurrence depends only on the spectral entanglement K. Moreover, Eq. (25) represents the largest concurrence obtainable from any of these source configurations. This point can be appreciated by noting that the solid curves in both panels of Fig. 5, i.e., the case $a=1$, correspond with Eq. (25).

IV. TYPE-I FUSION

We next analyze the role of spectral entanglement in the type-I fusion gate shown in Fig. 6. As in Sec. III, we consider the four-photon input state $|\Psi_{1234}\rangle=|\varphi_{12}\rangle|\varphi_{34}\rangle$. Photons 2 and 3 interfere at a polarizing beam splitter after which the output in path 2 is rotated by $\pi/4$ before detection with polarization discrimination. The action of the first PBS and the rotation of mode 2 by $\pi/4$ produces the four-photon state vector

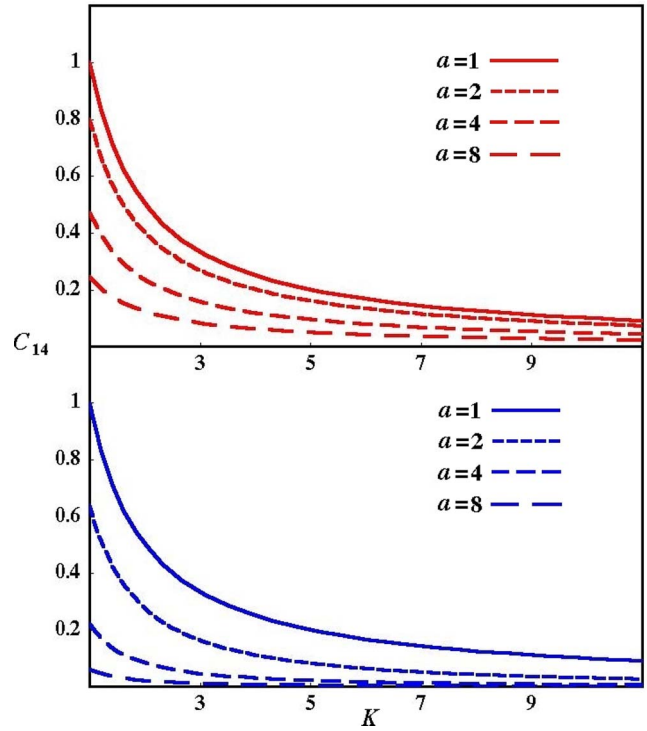

FIG. 5. (Color online) The concurrence C_{14} obtained after entanglement swapping as a function of the spectral entanglement K. The upper panel is the concurrence using the source configuration in Fig. 4(a), and the lower panel is the concurrence using the source configuration in Fig. 4(b). In each panel, the curves do not cross and are labeled in descending order by the value of the aspect ratio $a=\sigma/\sigma'$. For entanglement swapping the upper panel also quantifies the concurrence obtainable with the source configuration in Fig. 4(c). The solid line in both panels corresponds with the concurrence obtained from the source configuration in Fig. 4(d), which is independent of a.

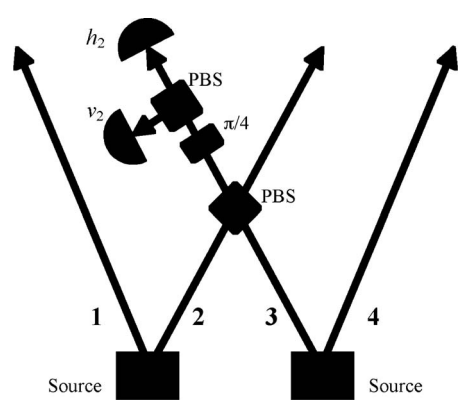

FIG. 6. A type-I fusion experiment where the interference of photons 2 and 3 at a polarizing beam splitter (PBS) is analyzed by rotating the output in mode 2 by $\pi/4$ and using a polarization beam splitter (PBS) and two detectors (h_2 and v_2). Single-photon detection events project photons 1, 3, and 4 into a linear cluster state. The black boxes signify the entangled photon sources and any additional linear optical elements.

$$|\Psi'_{1234}\rangle = \frac{1}{2}\int d\omega \int d\omega' \int d\bar{\omega} \int d\bar{\omega}'\{f_{12}(\omega,\omega')f_{34}(\bar{\omega},\bar{\omega}') \times|h_1(\omega),v_3(\omega'),h_3(\bar{\omega}),v_4(\bar{\omega}')\rangle + f_{12}(\omega,\omega')g_{34}(\bar{\omega},\bar{\omega}')|h_1(\omega),v_3(\omega'),h_4(\bar{\omega}')\rangle \times[|h_2(\bar{\omega})\rangle - |v_2(\bar{\omega})\rangle]/\sqrt{2} + g_{12}(\omega,\omega')f_{34}(\bar{\omega},\bar{\omega}') \times|v_1(\omega),h_3(\bar{\omega}),v_4(\bar{\omega}')\rangle[|h_2(\omega')\rangle + |v_2(\omega')\rangle]/\sqrt{2} + g_{12}(\omega,\omega')g_{34}(\bar{\omega},\bar{\omega}')|v_1(\omega),h_4(\bar{\omega}')\rangle[|h_2(\omega')\rangle + |v_2(\omega')\rangle][|h_2(\bar{\omega})\rangle - |v_2(\bar{\omega})\rangle]/2\}. \quad (26)$$

The second and third terms in the integrand of Eq. (26) contribute to single-photon detection events and the formation of a three-qubit cluster state. For the case of the projective measurement

$$\Pi(h_2) = \int |h_2(\omega)\rangle\langle h_2(\omega)|d\omega, \quad (27)$$

the resulting density matrix $\rho_{134}=\mathrm{Tr}_2[\Pi(h_2)\rho'_{1234}\Pi(h_2)]$ yields a normalized polarization density matrix

$$\tilde{\rho}_{134} = \frac{1}{2}(|h_1,v_3,h_4\rangle\langle h_1,v_3,h_4| + G_{134}|h_1,v_3,h_4\rangle\langle v_1,h_3,v_4| + G^*_{134}|v_1,h_3,v_4\rangle\langle h_1,v_3,h_4| + |v_1,h_3,v_4\rangle\langle v_1,h_3,v_4|) \quad (28)$$

with

$$G_{134} = \int d\omega \int d\omega' \int d\bar{\omega} \int d\bar{\omega}' f_{12}(\omega,\omega')g_{34}(\bar{\omega},\bar{\omega}') \times g_{12}(\omega,\bar{\omega})^* f_{34}(\omega',\bar{\omega}')^*. \quad (29)$$

A similar result is found when a single photon is detected in mode v_2.

Coffman, Kundu, and Wooters have shown how to quantify the entanglement of the tripartite state $\tilde{\rho}_{134}$ using the residual tangle [34]

$$\tau_{134} = C^2_{1(34)} - C^2_{13} - C^2_{14}, \quad (30)$$

where C_{13} and C_{14} are the concurrences of photon pairs (1,3) and (1,4), respectively, and $C_{1(34)}$ is the concurrence between photon 1 and the photon pair (3,4). It follows from Eq. (28) that $C_{13}=C_{14}=0$, as the corresponding bipartite density matrices are completely mixed. An analytic result for $C_{1(34)}$ exists when the (3,4) system is confined to a two-dimensional subspace, i.e., when the pair mimics a single qubit. This condition is satisfied here because of the specific form we have taken for the initially entangled input states. Therefore, by analogy with the concurrence of a bipartite density matrix, we have $\sqrt{\tau_{134}}=C_{1(34)}=|G_{134}|$.

We evaluate the behavior of $\sqrt{\tau_{134}}=C_{1(34)}$ with respect to the different source configurations in Fig. 4. When spectral differences correlate with polarization and $f^{\mathrm{pol}}_{12}(\omega,\omega')=f^{\mathrm{pol}}_{34}(\omega,\omega')$, as in source configuration (a), then

$$C^{(a)}_{1(34)} = C^{(b)}_{14}, \quad (31)$$

where $C^{(b)}_{14}$ was defined in Eq. (24). In contrast, when $f^{\mathrm{pol}}_{12}(\omega,\omega')=f^{\mathrm{pol}}_{34}(\omega',\omega)$, as in source configuration (b), then

$$C^{(b)}_{1(34)} = C^{(a)}_{14} \quad (32)$$

with $C^{(a)}_{14}$ given by Eq. (23). Consequently, the optimal source configuration for the fusion gate is reversed from the case of entanglement swapping. For comparison, when spectral differences correlate with path and the source configuration is either (c) $f^{\mathrm{path}}_{12}(\omega,\omega')=f^{\mathrm{path}}_{34}(\omega',\omega)$ or (d) $f^{\mathrm{path}}_{12}(\omega,\omega')=f^{\mathrm{path}}_{34}(\omega',\omega)$, the resulting concurrence is

$$C^{(c)}_{1(34)} = C^{(c)}_{14} = C^{(a)}_{14} \text{ and } C^{(d)}_{1(34)} = C^{(d)}_{14}, \quad (33)$$

respectively. Therefore, the results for the concurrence following type-I fusion are also portrayed by the curves in Fig. 5 with the distinction that the upper panel corresponds to source configuration (b) and the lower panel corresponds to source configurations (a) and (c). As with entanglement swapping, the solid curves in either panel corresponds to source configuration (d).

V. MULTIPLE SEQUENTIAL GATES

The above results for entanglement swapping and type-I fusion apply to the case that two pairs of entangled photons are used as input to the gates. A straightforward extension of these results considers the output from a serial sequence of each gate. Specifically, we calculate the biphoton states resulting from N sequential entanglement-swapping operations and the entangled $N+1$ photon states generated from N type-I fusion-gate operations acting on $2(N+1)$ initial photon pairs. In order to emphasize the role of spectral entanglement in the sequential gate operations, we neglect all other sources of error including the possibility that individual gates may fail. This simplification, which is not strictly necessary, provides a convenient context for understanding the specific effects of spectral entanglement on sequential gate operations.

For both entanglement swapping and fusion, we assume the initial state is an even number of $N/2=(n+1)$ polarization-entangled photon pairs and $|\Psi_{1\cdots N}\rangle = |\varphi_{12}\rangle\cdots|\varphi_{N-1,N}\rangle$. We model the n measurements made by either protocol following the prescriptions outlined in the prior sections. The biphoton state resulting from n entanglement swapping events leads to the polarization density matrix

$$\tilde{\rho}_{1,N} = \frac{1}{2}(|h_1,v_N\rangle\langle h_1,v_N| + G_{1,N}|h_1,v_N\rangle\langle v_1,h_N| + G^*_{1,N}|v_1,h_N\rangle\langle h_1,v_N| + |v_1,h_N\rangle\langle v_1,h_N|), \quad (34)$$

where

$$G_{1,N}=\int dx\int dy\left[\int d\mathbf{z}f_{12}(x,z_1)g_{34}(z_1,z_2)^*f_{56}(z_2,z_3)\cdots g_{N-1,N}(z_n,y)^*\right]\left[\int d\mathbf{z}g_{12}(x,z_1)^*f_{34}(z_1,z_2)g_{56}(z_2,z_3)^*\cdots f_{N-1,N}(z_n,y)\right]. \tag{35}$$

Likewise, the polarization density matrix after n sequential type-I fusion gates is

$$\tilde{\rho}_{1,3,5,\ldots,N}=\frac{1}{2}(|h_1,v_3,h_5,\ldots,v_N\rangle\langle h_1,v_3,h_5,\ldots,v_N|+G_{1,3,5,\ldots,N}|h_1,v_3,h_5,\ldots,v_N\rangle\langle v_1,h_3,v_5,\ldots,h_N|$$
$$+G^*_{1,3,5,\ldots,N}|v_1,h_3,v_5,\ldots,h_N\rangle\langle h_1,v_3,h_5,\ldots,v_N|+|v_1,h_3,v_5,\ldots,h_N\rangle\langle v_1,h_3,v_5,\ldots,h_N|), \tag{36}$$

where

$$G_{1,3,5,\ldots,N}=\int dx\int dy\left[\int d\mathbf{z}f_{12}(x,z_1)f_{34}(z_1,z_2)^*f_{56}(z_2,z_3)\ldots f_{N-1,N}(z_n,y)^*\right]$$
$$\times\left[\int d\mathbf{z}g_{12}(x,z_1)^*g_{34}(z_1,z_2)g_{56}(z_2,z_3)^*\ldots g_{N-1,N}(z_n,y)\right] \tag{37}$$

and $N/2-1$ photons contribute to Eq. (36). Similar results are obtained for both protocols in the case of an odd number of initial photon pairs.

The density matrices of Eqs. (34) and (36) describe different physical states and they depend on the coherence elements defined by Eqs. (35) and (37), respectively. When $f_{ij}(\omega,\omega')=g_{ij}(\omega,\omega')$ for all i and j, however, these coherences become identical and $G_{1,N}=G_{1,3,5,\ldots,N}=G$. If the $N/2$ entanglement sources are configured according to the prescription of Fig. 4(d), then the largest obtainable coherence can be determined using the Schmidt decomposition of the common joint spectral amplitude. This leads to the result that $C=|G|$ is

$$C=\sum_{j=0}^{\infty}\lambda_j^{N/2}. \tag{38}$$

Substituting the Schmidt coefficients from Eq. (9) yields

$$C=\frac{\operatorname{sech}^N\varphi}{1-\tanh^N\varphi}. \tag{39}$$

In Fig. 7, C is plotted as a function of the angle φ for incremental values of $N=1$ to 8.

VI. CONCLUSIONS

Type-I fusion with polarization-entangled photons maximizes the residual tangle when the interfering photons (2 and 3) are mode matched and spectrally unentangled. An identical condition is found for maximizing the bipartite concurrence with entanglement swapping. These considerations are portrayed by source configuration (d), which approaches the theoretical idealization of polarization-encoded qubits only in the limit the photons are spectrally unentangled. The presence of entanglement in the initial joint spectral amplitude lowers the concurrence obtainable with either protocol, as summarized by Eq. (25) and demonstrated by the solid curves in Fig. 5.

On the other hand, when spectral differences correlate with polarization the entanglement obtained from entanglement swapping and type-I fusion depends on how the sources are configured. For entanglement swapping source configuration (a) leads to a larger concurrence than source configuration (b), while the converse statement is true for type-I fusion. The basis for this distinction lies in the different detection strategies of the two protocols. Both protocols perform best when there is an absence of which-path information. For entanglement swapping, if the oppositely polarized photons with different spectra in source configuration (a) meet at the beam splitter, then monitoring the frequency and polarization of the detected photons does not distinguish between the two interference processes, e.g., h_3 transmitted and v_2 reflected versus h_2 reflected and v_3 transmitted. If, however, the oppositely polarized photons having identical spectra in source configuration (b) meet at the beam splitter, then the source of each photon can be determined by detecting the frequency and polarization of the photons.

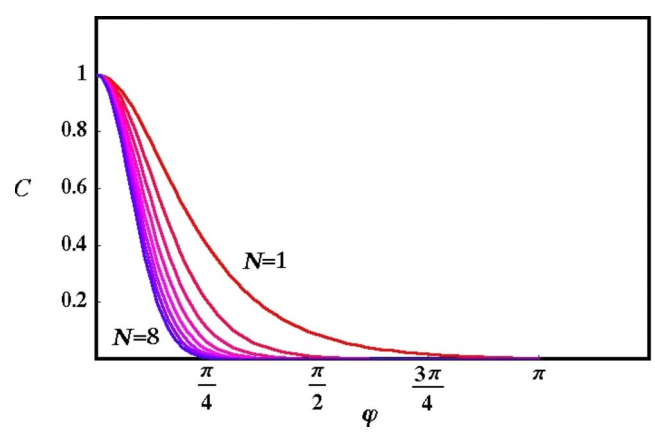

FIG. 7. (Color online) The coherence magnitude C versus the angle φ and the number of sequential gate operations N. The curves are labeled by the number of gate operations $N=1$ to 8 and represent the results both of entanglement swapping and type-I fusion.

In the case of type-I fusion, the parity-check measurement erases the polarization information pertaining to the incident photon before detection. The erasure step works best with source configuration (b), where oppositely polarized photons are spectrally identical. This is because monitoring the frequency as well as the polarization of the detected photon does not permit one to distinguish between the relevant interference processes, i.e., whether two vertical or two horizontal photons meet at the polarizing beam splitter. If the oppositely polarized photons with different spectra from source configuration (a) were to pass through the polarizing beam splitter, then the input to the polarization rotator in mode 2 could be determined based on the frequency of the detected photon.

Source configurations (a) and (b) cannot maximize the concurrence of the entangled states prepared with these protocols. Despite optimizing the interference process, photons 1 and 4 necessarily carry distinguishing information in the correlations between the polarization and spectral degrees of freedom. Indeed, it was this same information that led to the less-than-unit concurrence of the initial photon pairs, cf. Fig. 2. In contrast, source configurations (c) and (d) are free from cross correlations between spectra and polarization, and the initial photon pairs produced with these sources have maximal concurrence. However, source configuration (c) does not optimize the Bell-state measurement or the quantum-eraser technique because the marginal spectra of the photons are not identical. As a result the obtainable concurrence with source configuration (c) is always reduced relative to the concurrences of the initial photon pairs.

Our consideration of spectral entanglement has also been extended to the case of sequential gates. The curves in Fig. 7 portray the progressive loss in polarization entanglement as the number of gates and the amount of spectral entanglement (expressed in terms of φ) increases. The present analysis has left open the question of how spectral entanglement will impact entanglement distillation [35], which may also improve the performance of sequential entanglement swapping in the current context, or how redundant encoding in cluster preparation [20] will impact the performance of the (type-I) fusion gates when using multimode qubits. We also have not investigated the differences between gates based on polarization entanglement and gates based on hyperentanglement [13–16], but we anticipate that the present analysis will be useful for comparing the concurrence obtainable by these different approaches, especially for the case of finite spectral entanglement.

In summary, we have derived expressions for the bipartite concurrence and the residual tangle resulting from entanglement swapping and type-I fusion, respectively, when using spectrally multimode photons. In particular, we have established the impact that spectral entanglement has on the success of these polarization-based protocols for generating polarization-entangled states. These considerations should prove useful in the design of future broad-bandwidth polarization-entanglement sources for implementing quantum information protocols.

[1] P. G. Kwiat, K. Mattle, H. Weinfurter, A. Zeilinger, A. V. Sergienko, and Y. Shih, Phys. Rev. Lett. **75**, 4337 (1995); P. G. Kwiat, E. Waks, A. G. White, I. Appelbaum, and P. H. Eberhard, Phys. Rev. A **60**, R773 (1999).

[2] T. S. Humble and W. P. Grice, Phys. Rev. A **75**, 022307 (2007).

[3] C. K. Law, I. A. Walmsley, and J. H. Eberly, Phys. Rev. Lett. **84**, 5304 (2000).

[4] W. P. Grice, A. B. U'Ren, and I. A. Walmsley, Phys. Rev. A **64**, 063815 (2001).

[5] C. K. Law and J. H. Eberly, Phys. Rev. Lett. **92**, 127903 (2004).

[6] A. B. U'Ren, K. Banaszek, and I. A. Walmsley, Quantum Inf. Comput. **3**, 480 (2003).

[7] J. P. Torres, M. W. Mitchell, and M. Hendrych, Phys. Rev. A **71**, 022320 (2005).

[8] Y.-H. Kim and W. P. Grice, Phys. Rev. A **68**, 062305 (2003).

[9] D. Branning, W. P. Grice, R. Erdmann, and I. A. Walmsley, Phys. Rev. Lett. **83**, 955 (1999).

[10] V. Giovannetti, L. Maccone, J. H. Shapiro, and F. N. C. Wong, Phys. Rev. Lett. **88**, 183602 (2002).

[11] A. B. U'Ren, R. K. Erdmann, M. de la Cruz-Gutierrez, and I. A. Walmsley, Phys. Rev. Lett. **97**, 223602 (2006).

[12] S. Carrasco, A. Sergienko, B. E. A. Saleh, M. C. Teich, J. P. Torres, and L. Torner, Phys. Rev. A **73**, 063802 (2006).

[13] P. G. Kwiat, J. Mod. Opt. **44**, 2173 (1997).

[14] J. T. Barreiro, N. K. Langford, N. A. Peters, and P. G. Kwiat, Phys. Rev. Lett. **95**, 260501 (2005).

[15] P. G. Kwiat and H. Weinfurter, Phys. Rev. A **58**, R2623 (1998).

[16] T.-C. Wei, J. T. Barreiro, and P. G. Kwiat, Phys. Rev. A **75**, 060305(R) (2007).

[17] C. H. Bennett, G. Brassard, C. Crepeau, R. Jozsa, A. Peres, and W. K. Wootters, Phys. Rev. Lett. **70**, 1895 (1993).

[18] E. Knill, R. Laflamme, and G. J. Milburn, Nature (London) **409**, 46 (2001).

[19] W. Dür, H.-J. Briegel, J. I. Cirac, and P. Zoller, Phys. Rev. A **59**, 169 (1999).

[20] D. E. Browne and T. Rudolph, Phys. Rev. Lett. **95**, 010501 (2005).

[21] T. B. Pittman, B. C. Jacobs, and J. D. Franson, Phys. Rev. A **64**, 062311 (2001); Phys. Rev. Lett. **88**, 257902 (2002).

[22] H. J. Briegel and R. Raussendorf, Phys. Rev. Lett. **86**, 910 (2001).

[23] R. Raussendorf and H. J. Briegel, Phys. Rev. Lett. **86**, 5188 (2001).

[24] W. P. Grice and I. A. Walmsley, Phys. Rev. A **56**, 1627 (1997).

[25] Y. Nambu, K. Usami, Y. Tsuda, K. Matsumoto, and K. Nakamura, Phys. Rev. A **66**, 033816 (2002).

[26] S. Parker, S. Bose, and M. B. Plenio, Phys. Rev. A **61**, 032305 (2000).

[27] R. Erdmann, D. Branning, W. Grice, and I. A. Walmsley, Phys.

Rev. A **62**, 053810 (2000).

[28] R. Grobe, K. Rzazewski, and J. H. Eberly, J. Phys. B **27**, L503 (1995).

[29] The Schmidt decomposition of the bivariate Gaussian is obtained by using the substitutions $\tanh\varphi=2t$ in Mehler's formula $(1-4t^2)^{-1/2}\exp[\{4xyt-4t^2(x^2+y^2)\}/(1-4t^2)] =\sum_{n=0}^{\infty}H_n(x)H_n(y)t^n/n!$. The latter can be found in P. M. Morse and H. Feshbach, *Method of Theoretical Physics* (McGraw-Hill, New York, 1953).

[30] W. K. Wootters, Phys. Rev. Lett. **80**, 2245 (1998).

[31] S. L. Braunstein and A. Mann, Phys. Rev. A **51**, R1727 (1995).

[32] P. P. Rohde and T. C. Ralph, J. Mod. Opt. **53**, 1589 (2006).

[33] Coincidences between detectors (h_2, h_3) and (v_2, v_3), or the two-photon detection events given by (h_2, h_2), (h_3, h_3), (v_2, v_2), and (v_3, v_3), do not lead to an entangled state for photons 1 and 4. Modeling these two-photon detection events requires introduction of a factor of $\frac{1}{2}$ into the definition of the projection operator to ensure idempotency.

[34] V. Coffman, J. Kundu, and W. K. Wootters, Phys. Rev. A **61**, 052306 (2000).

[35] C. H. Bennett, H. J. Bernstein, S. Popescu, and B. Schumacher, Phys. Rev. A **53**, 2046 (1996).